ACCURACY OF RADIAL BASIS FUNCTION INTERPOLATION AND DERIVATIVE APPROXIMATIONS ON 1-D INFINITE GRIDS

BENGT FORNBERG* AND NATASHA FLYER†

Abstract. Radial basis function (RBF) interpolation can be very effective for scattered data in any number of dimensions. As one of their many applications, RBFs can provide highly accurate collocation-type numerical solutions to several classes of PDEs. To better understand the accuracy that can be obtained, we survey here derivative approximations based on RBFs using a similar Fourier analysis approach that has become the standard way for assessing the accuracy of finite difference schemes. We find that the accuracy is directly linked to the decay rate, at large arguments, of the (generalized) Fourier transform of the radial function. Three different types of convergence rates can be distinguished as the node density increases - polynomial, spectral, and super-spectral, as exemplified for example by thin plate splines, multiquadrics, and Gaussians respectively.

1. Introduction. Many applications lead to the problem of interpolating data y_k at scattered locations $\underline{x}_k \in R^d$, $k = 1, 2, ...n$. In the most straightforward radial basis function (RBF) approach to this task, we construct an interpolant of the form

$$s(\underline{x}) = \sum_{k=1}^{n} \lambda_k \ \phi(\|\underline{x} - \underline{x}_k\|) \tag{1.1}$$

where $\|\cdot\|$ denotes Euclidean distance, and $\phi(r)$ is some *radial function*. The expansion coefficients λ_k are determined so that $s(\underline{x}_k) = y_k$. The primary choice in the implementation is what function $\phi(r)$ to use. Some of the most common choices are listed in Table 1.1. They all feature a free parameter. For the piecewise smooth cases, n is usually selected as $n = 1$ or $n = 2$, whereas the best choice for the shape parameter ε in the smooth cases has been subject to extensive study. (e.g. [4], [6], [19]).

Once a smooth interpolant $s(\underline{x})$ to the scattered data has been found, it becomes possible to differentiate it and thereby obtain accurate approximations to partial derivatives. The use of such approximations for the numerical solution of PDEs was pioneered around 1990 by E. Kansa for elliptic, parabolic, and certain hyperbolic problems [12], [13]. This approach has similarities to how finite difference (FD) formulas are obtained, but with some differences:

- FD formulas are typically obtained by differentiating polynomial interpolants (rather than RBF type interpolants),
- Most FD formulas (stencils) extend only over a small subset of the data points, local to the position at which the derivative approximation is sought.

If one includes increasingly many data points in 1-D FD formulas, one obtains, in the limit, a spectral method (as shown in [7]). For example:

- With periodic equi-spaced data, FD stencils with widths tending to infinity will reproduce the Fourier pseudospectral (Fourier PS) method,
- With data on a finite interval located at Chebyshev / Legendre / Jacobi node points, global FD approximations will reproduce the corresponding polynomial PS methods.

Radial function $\phi(r)$, $r \geq 0$	Name
Piecewise Smooth	
r^{2n-1}, $n = 1, 2, 3, \ldots$	Powers (linear, cubic, quintic, ...)
$r^{2n} \ln r$, $n = 1, 2, 3, \ldots$	Thin Plate Splines (TPS)
Infinitely Smooth	
$\dfrac{1}{1 + (\varepsilon r)^2}$	Inverse Quadratic (IQ)
$\sqrt{1 + (\varepsilon r)^2}$	Multiquadric (MQ)
$e^{-(\varepsilon r)^2}$	Gaussian (GA)

<div align="center">TABLE 1.1</div>

Some common types of radial functions $\phi(r)$ for RBFs $\phi(\|\underline{x} - \underline{x}_k\|)$. The smoothness refers to the functions when extended to negative arguments as even functions, i.e. $\phi(-r) = \phi(r)$.

Since PS methods can offer superior accuracy and cost effectiveness in simple geometries, there has been great interest in generalizing them to irregular geometries (for example by means of introducing spectral elements). By basing PS methods on RBF interpolants rather than on polynomial or trigonometric ones, generalizations to irregular domains and node distributions can be both simple and highly effective, as demonstrated in the case of Poisson's equation in 2-D, [14].

The purpose of the present paper is to add to the understanding of the accuracy and convergence rates that can be expected from RBF type interpolants, by means of analyzing them in the special case of an equi-spaced periodic 1-D grid. We will use Fourier analysis to study the accuracy of RBF interpolants to trigonometric functions, and compare the first derivative approximations against the ones obtained by FD methods, presenting the results in the manner that has become standard in the FD literature. Some of the RBF observations in this paper can be extracted from formulas given, although in different contexts, in papers such as [2] and [3] This study differs in that it

- Provides a number of novel closed-form expressions for RBF sums, and
- Uses these to compare RBF approximations against FD and spectral methods for derivative approximations.

2. RBF expansion coefficients when interpolating trigonometric data. The first step in obtaining the interpolant $s(x)$ to trigonometric data is to find the RBF expansion coefficients λ_k. In the next two subsections, we obtain a general formula for these coefficients in terms of Poisson sums. We then determine the Poisson sums for the main types of radial functions.

2.1. Formula for the RBF expansion coefficients in terms of the Fourier transform of the radial functions. The RBF expansion of a function $f(x)$ on an infinite 1D grid of spacing h becomes

$$f(nh) = \sum_{k=-\infty}^{\infty} \lambda_k \phi(|nh - kh|) \quad , \quad n \epsilon Z \ . \tag{2.1}$$

In the following, we will asume that the radial functions $\phi(r)$ are extended to negative arguments as even functions of r, and we will omit the magnitude operator in the arguments of ϕ. The sum in (2.1) can be viewed as a discrete convolution which, in

Fourier space, can be written as

$$\sum_{n=-\infty}^{\infty} f(nh)e^{-inh\xi} = \sum_{n=-\infty}^{\infty} \left(\sum_{k=-\infty}^{\infty} \lambda_k \phi(nh - kh) \right) e^{-inh\xi} \tag{2.2}$$

$$= \left(\sum_{k=-\infty}^{\infty} \lambda_k e^{-ikh\xi} \right) \left(\sum_{m=-\infty}^{\infty} \phi(mh)e^{-imh\xi} \right). \tag{2.3}$$

Thus, we can write down the expansion coefficients explicitly

$$\lambda_k = \frac{h}{2\pi} \int_{\frac{-\pi}{h}}^{\frac{\pi}{h}} \frac{\sum_{n=-\infty}^{\infty} f(nh)e^{-inh\xi}}{\sum_{m=-\infty}^{\infty} \phi(mh)e^{-imh\xi}} e^{ikh\xi} d\xi. \tag{2.4}$$

For $[-\pi, \pi]$−periodic Fourier data, $f(nh) = e^{i\omega nh}$, where $-\frac{\pi}{h} \leq \omega \leq \frac{\pi}{h}$ (representing the largest range of frequencies that can exist on a grid with spacing h). The numerator of the integrand of (2.4) then reduces to

$$\sum_{n=-\infty}^{\infty} f(nh)e^{-inh\xi} = \frac{2\pi}{h}\delta(\omega - \xi), \tag{2.5}$$

resulting in

$$\lambda_k = \frac{e^{i\omega hk}}{\Xi(\omega, h)} \tag{2.6}$$

where

$$\Xi(\omega, h) = \sum_{m=-\infty}^{\infty} \phi(mh)e^{-i\omega mh} \tag{2.7}$$

Thus, the expansion coefficients λ_k are proportional to $e^{i\omega hk}$, and are scaled by the coefficients of the discrete Fourier transform of the RBF. This transform can be found by summing the continuous Fourier transform over a $\frac{2\pi}{h}$−periodic grid (a Poisson sum; [15]):

$$\Xi(\omega, h) = \frac{1}{h} \sum_{j=-\infty}^{\infty} \hat{\phi}(\omega + \frac{2\pi j}{h}) \tag{2.8}$$

where

$$\hat{\phi}(\omega) = \int_{-\infty}^{\infty} \phi(y)e^{-i\omega y}dy. \tag{2.9}$$

Therefore, we can also express λ_k in terms of the continuous Fourier transform as

$$\lambda_k = \frac{e^{i\omega hk}}{\frac{1}{h} \sum_{j=-\infty}^{\infty} \hat{\phi}(\omega + \frac{2\pi j}{h})}. \tag{2.10}$$

3

RBF $\phi(r)$	Fourier transform $\hat{\phi}(\omega)$	Poisson Sum $\Xi(\omega, h)$
r	$-\frac{2}{\omega^2}$	$\frac{-h}{2\sin(\frac{\omega h}{2})^2}$
r^3	$\frac{12}{\omega^4}$	$\frac{h^3(2+\cos\omega h)}{4(\sin\frac{\omega h}{2})^4}$
r^{2n-1}	$\frac{2(-1)^n(2n-1)!}{(\omega)^{2n}}$	$(-1)^n\frac{d^{2n-1}}{d\omega^{2n-1}}\cot(\frac{\omega h}{2})$
$r^2\ln r$	$\frac{4\pi}{|\omega|^3}$	$-\frac{h^3\left[\Psi^{(2)}(\frac{\omega h}{2\pi})+\Psi^{(2)}(1-\frac{\omega h}{2\pi})\right]}{4\pi^2}$
$r^{2n}\ln r$	$(-1)^{n+1}\frac{(2n)!2\pi}{|\omega|^{2n+1}}$	$\left(\frac{ih}{2\pi}\right)^{2n}\frac{\left[\Psi^{(2n)}(\frac{\omega h}{2\pi})+\Psi^{(2n)}(1-\frac{\omega h}{2\pi})\right]}{2}$
$\frac{1}{1+(\varepsilon r)^2}$	$\frac{\pi}{\varepsilon}e^{\frac{-|\omega|}{\varepsilon}}$	$\frac{\pi\cosh(\frac{\omega h-\pi}{\varepsilon h})}{\varepsilon h\sinh(\frac{\pi}{\varepsilon h})}$
$\frac{1}{1+(\varepsilon r)^{2n}}$	computed directly via (2.7)	$\frac{\pi}{2n\varepsilon h}\sum_{j=1}^{2n}\frac{e^{\frac{-i\omega}{\varepsilon\alpha(j)}}}{\alpha(j)}[\cot\frac{\pi}{\varepsilon h\alpha(j)}+\text{sign}(\omega)i]$, where $\alpha(j)=e^{(i\pi\frac{2j-1}{2n})}$
$\sqrt{1+(\varepsilon r)^2}$	$\frac{-2K_1(\frac{|\omega|}{\varepsilon})}{\epsilon|\omega|}$	$-\frac{2}{\epsilon h}\sum_{j=-\infty}^{\infty}\frac{K_1(\frac{1}{\varepsilon}|\omega+\frac{2\pi}{h}j|)}{|\omega+\frac{2\pi}{h}j|}$
$e^{-(\varepsilon r)^2}$	$\frac{\sqrt{\pi}}{\varepsilon}e^{-\frac{\omega^2}{4\varepsilon^2}}$	$\frac{\sqrt{\pi}}{\varepsilon h}\sum_{j=-\infty}^{\infty}e^{-\frac{(\omega h+2\pi j)^2}{4\varepsilon^2 h^2}}$

TABLE 2.1
The Fourier transform and Poisson sums for different radial functions $\phi(r)$

2.2. Fourier transforms and Poisson sums of different RBFs. In cases where $\phi(r)$ goes to zero sufficiently fast as $r \to \infty$ (e.g. IQ and GA; cf Table 1.1), the Fourier transform $\hat{\phi}(\xi)$ is uniquely determined by (2.9). In other cases (e.g. MQ, TPS, powers, etc.), it becomes necessary to employ generalized Fourier transforms ([11], [15]) in place of (2.9). In the present context, these can be used in (2.10) just like regular Fourier transforms similarly to how they have been used previously for analyzing cardinal RBF interpolants (e.g. [1], [3], [10], [16]). The Fourier transforms (generalized, if needed), together with the corresponding Poisson sums $\Xi(\xi, h)$, are given in Table 2.1 for a selection of different radial functions $\phi(r)$. Below are some notes on the table:

- In the formulas for $\phi(r) = r^2\ln r$ and $\phi(r) = r^{2n}\ln r$, the function $\Psi^{(n)}(z)$ denotes the polygamma function, defined by $\Psi^{(n)}(z) = \frac{d^{n+1}}{dz^{n+1}}\ln\Gamma(z)$.
- The Poisson sum that is given for $\phi(r) = e^{-(\varepsilon r)^2}$, obtained from (2.8), converges much more rapidly for small ε than $\Xi(\xi, h) = \sum_{j=-\infty}^{\infty} e^{-(\varepsilon h j)^2}e^{-i\xi h j}$ (which follows from (2.7)).
- Although radial functions of the form $\phi(r) = 1/(1 + (\varepsilon r)^{2n})$, $n = 1, 2, 3, \ldots$ are included for the sake of generality, it should be noted that, as n increases, these RBFs begin to resemble step functions and thus become very poor interpolants.

4

3. RBF interpolation of Fourier data. In this section, we note that closed-form expressions can often be found for the RBF interpolants to Fourier data. In cases where the infinite sums that arise cannot be evaluated in closed form (such as with MQ and GA), we can nevertheless obtain simple and accurate estimates of the interpolation error. These will be used to relate the decay rate of the Fourier transform of $\phi(r)$ to the rate of convergence of the RBF interpolants.

3.1. An alternative expression for the RBF interpolant. It follows from (2.1) and (2.6) that the RBF interpolant to the trigonometric mode $e^{i\omega x}$ can be written as

$$s(x) = \frac{1}{\Xi(\omega, h)} \sum_{j=-\infty}^{\infty} \phi(x - hj)e^{i\omega hj}. \tag{3.1}$$

This formula is of limited utility, since it diverges if $\phi(r)$ grows as $r \to \infty$. Invoking the generalized Fourier transform circumvents this difficulty. The starting point is then to view the summation in (3.1) as a discrete Fourier transform, and let that be represented via a continuous Fourier transform summed over a $\frac{2\pi}{h}$ grid (again a Poisson sum):

$$\sum_{j=-\infty}^{\infty} \phi(x - hj)e^{i\omega hj} = \frac{1}{h} \sum_{j=-\infty}^{\infty} \int_{-\infty}^{\infty} \phi(x - y) e^{i(\omega + \frac{2\pi j}{h})y}dy.$$

By the commutative law for convolutions we have

$$\sum_{j=-\infty}^{\infty} \phi(x - hj)e^{i\omega hj} = \frac{1}{h} \sum_{j=-\infty}^{\infty} \int_{-\infty}^{\infty} \phi(y)e^{i(\omega + \frac{2\pi j}{h})(x-y)}dw$$

$$= \frac{1}{h} \sum_{j=-\infty}^{\infty} \hat{\phi}(\omega + \frac{2\pi j}{h})e^{i(\omega + \frac{2\pi j}{h})x} ,$$

i.e. the interpolant becomes

$$s(x) = \frac{\sum_{j=-\infty}^{\infty} \hat{\phi}(\omega + \frac{2\pi j}{h})e^{i(\omega + \frac{2\pi j}{h})x}}{h\Xi(\omega, h)} \tag{3.2}$$

To obtain the RBF interpolant for $\cos(\omega x)$ (rather than for $e^{i\omega x}$), we take the real part of (3.2):

$$s(x) = \frac{1}{\sum_{j=-\infty}^{\infty} \hat{\phi}(\omega + \frac{2\pi j}{h})} \sum_{j=-\infty}^{\infty} \hat{\phi}(\omega + \frac{2\pi j}{h}) \cos\left((\omega + \frac{2\pi j}{h})x\right). \tag{3.3}$$

In contrast to (3.1), convergence now depends only on the smoothness of $\phi(r)$ (which for this purpose is sufficient in all cases that we are studying), and not on whether $\phi(r)$ decays or grows for large r.

It follows from (3.3) that, if $\hat{\phi}(\xi)$ decreases exponentially fast with ξ, spectral convergence will result when $h \to 0$. This is the case for infinitely smooth RBFs, such as IQ, MQ, and GA.

RBF $\phi(x)$	Interpolant $s(x)$ to $\cos\omega x$
r^{2n-1}	$\dfrac{\mathrm{Re}\left(e^{i\omega x}\frac{\partial^{2n-1}}{\partial\omega^{2n-1}}\left[\left(\cot\frac{\omega h}{2}+i\right)e^{i\omega h\left\{\frac{x}{h}\right\}}\right]\right)}{\frac{\partial^{2n-1}}{\partial\omega^{2n-1}}\cot\frac{\omega h}{2}}$
$r^{2n}\ln r$	$\begin{aligned}\mathrm{Re}&\left(e^{i\omega x}\left[\frac{1}{|\omega|^{2n+1}}+\left(\frac{h}{2\pi}\right)^{2n+1}\right.\right.\\&\times\left(e^{i\frac{2\pi x}{h}}\left(\Phi(e^{i\frac{2\pi x}{h}},2n+1,1+\frac{\omega h}{2\pi})\right)\right.\\&\left.\left.\left.+e^{-i\frac{2\pi x}{h}}\left(\Phi(e^{-i\frac{2\pi x}{h}},2n+1,1-\frac{\omega h}{2\pi})\right)\right)\right]\right)\end{aligned}$
$\dfrac{1}{1+(\varepsilon r)^2}$	$\dfrac{\cos\omega x\,\sinh\frac{2\pi-\omega h}{\varepsilon h}+\cos(\omega x-\frac{2\pi x}{h})\sinh\frac{\omega}{\varepsilon}}{(\cosh\frac{2\pi}{\varepsilon h}-\cos\frac{2\pi x}{h})(\cosh(\frac{\omega}{\varepsilon})\coth(\frac{\pi}{\varepsilon h})-\sinh(\frac{\omega}{\varepsilon}))}$
$\sqrt{1+(\varepsilon r)^2}$	$\dfrac{\sum_{j=-\infty}^{\infty}\frac{K_1(\frac{1}{\varepsilon h}|\omega h+2\pi j|)}{|\omega h+2\pi j|}\cos(\omega+\frac{2\pi j}{h})x}{\sum_{j=-\infty}^{\infty}\frac{K_1(\frac{1}{\varepsilon h}|\omega h+2\pi j|)}{|\omega h+2\pi j|}}$
$e^{-(\varepsilon r)^2}$	$\dfrac{\sum_{j=-\infty}^{\infty}e^{-\left(\frac{\omega h+2\pi j}{2\varepsilon h}\right)^2}\cos(\omega+\frac{2\pi j}{h})x}{\sum_{j=-\infty}^{\infty}e^{-\left(\frac{\omega h+2\pi j}{2\varepsilon h}\right)^2}}$

TABLE 3.1

The interpolant $s(x)$ to $\cos(\omega x)$ for different radial functions $\phi(r)$

3.2. Closed form expressions for the RBF interpolants to $\cos\omega x$. Closed form expressions for the interpolant $s(x)$ (as given by (3.3)) can be derived in several cases, such as powers, TPS, and IQ. In the cases of MQ and GA, we cannot sum (3.3) in closed form, but that is of little consequence. In all cases when $\phi(r)$ is smooth, the sum in (3.3) converges extremely fast, and only the first terms (with $j=0$, ±1) need to be considered in order to find the leading error. Table 3.1 summarizes these formulas for the interpolants $s(x)$ to $\cos\omega x$ in cases of different radial functions $\phi(r)$. A couple of notational comments:

- For $\phi(r)=r^{2n-1}$, the symbol $\left\{\frac{x}{h}\right\}$ denotes the fractional part of the argument (i.e. $\left\{\frac{x}{h}\right\}=\frac{x}{h}-\left[\text{nearest integer}\le\frac{x}{h}\right]$).
- For $\phi(r)=r^{2n}\ln r$, the symbol Φ denotes the Lerch transcendental function, defined as $\Phi(z,s,a)=\sum_{k=0}^{\infty}\frac{z^k}{(a+k)^s}$.

In the summation in (3.3), the $j=0$ term recovers the trigonometric mode $\cos\omega x$ (albeit with a slightly wrong amplitude), and the $j=\pm1$ terms give a higher frequency correction, such that the interpolation conditions can be met at all the nodes.

Figure 3.1 illustrates the interpolation errors for different choices of $\phi(r)$ in the case of $\omega=1$ and $n=12$, i.e. $h=2\pi/n$. In the IQ, MQ, and GA cases, the shape parameter is set to $\varepsilon=1$. The solid curves in Figure 3.1 show the true interpolation errors, according to the formulas in Table 3.1 (with the interpolation points marked by dots - the errors of course being zero at these locations). The dashed curves show the approximation for the error we get if we include only the $j=0$ term in (3.3). We denote these $j=0$ errors (small multiples of $\cos\omega x$) as the *leading mean errors*.

It is interesting to note that the RBF interpolation error is of a somewhat different structure than what is typical for polynomial and trigonometric interpolation. In those cases, the error usually oscillates locally around a zero mean rather than around a
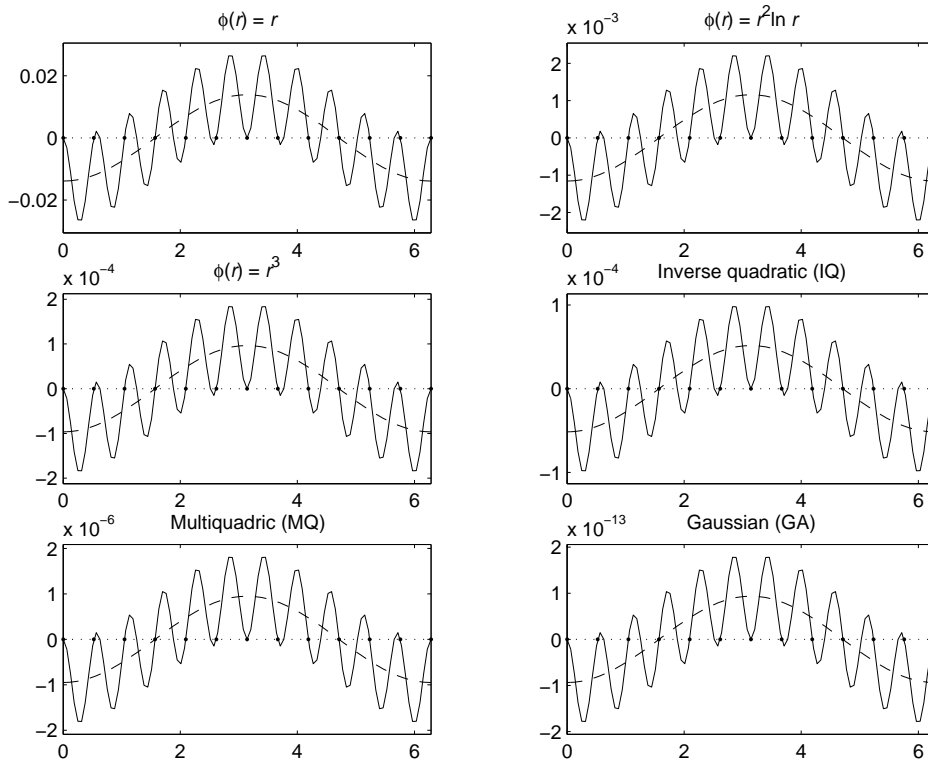
FIG. 3.1. *The true error (solid) and the leading mean error (dashed) in approximating $\cos \omega x$ in the case of $\omega = 1$, $n = 12$, i.e. $h = 2\pi/n$. In the IQ, MQ, and GA cases, the shape parameter $\varepsilon = 1$. The dots mark were the errors are zero due to the interpolation conditions.*

curve that is a very small multiple of the function being interpolated.

3.3. Comparison between the RBF interpolation errors when $h \to 0$ and when $\varepsilon \to 0$. The order of accuracy of a method refers to the rate by which the error decreases to zero when the grid spacing $h \to 0$. When using smooth RBFs, we also have the shape parameter ε present. The influence of ε on the accuracy is less intuitively clear. We are here interested in analyzing the error both as $h \to 0$ and (separately) $\varepsilon \to 0$. In the present case of interpolating very smooth (trigonometric) functions, we will see that the effects of $h \to 0$ and $\varepsilon \to 0$ are very similar. Figure 3.1 shows the interpolation errors when $\varepsilon = 1$ and h is quite small. Although the curves in the different subplots look similar, the scales on the vertical axes are vastly different. To approximate the amplitude of the leading mean error, we simply need to take the three central terms ($j = 0, \pm 1$) in (2.8) (for the Poisson sum) and the $j = 0$ term of the summation given in (3.3). Both as $h \to 0$ and as $\varepsilon \to 0$, the amplitude of the leading mean errors (denoted by $g_h(\omega, \varepsilon, h)$ and $g_\varepsilon(\omega, \varepsilon, h)$, respectively), are obtained by

Radial function $\phi(r)$	$g_h(\omega,\varepsilon,h)$	$g_\varepsilon(\omega,\varepsilon,h)$
r^{2n-1}	$2\left(\frac{\omega h}{2\pi}\right)^{2n}$	—
$r^{2n}\ln r$	$2\left(\frac{\omega h}{2\pi}\right)^{2n+1}$	—
$\frac{1}{1+(\varepsilon r)^2}$	$e^{-\frac{2\pi}{\varepsilon h}}\left(1+e^{\frac{2\omega}{\varepsilon}}\right)$	$e^{-\frac{2(\pi-\omega h)}{\varepsilon h}}$
$\sqrt{1+(\varepsilon r)^2}$	$e^{-\frac{2\pi}{\varepsilon h}}\left[\frac{\sqrt{\varepsilon}\omega h^{3/2}}{K_1(\frac{\omega}{\varepsilon})2\pi}\cosh(\frac{\omega}{\varepsilon})\right]$	$e^{-\frac{2(\pi-\omega h)}{\varepsilon h}}\sqrt{\omega h}\left[\left(\frac{1}{2\pi-\omega h}\right)^{3/2}\right]$
$e^{-(\varepsilon r)^2}$	$e^{-\frac{\pi}{(\varepsilon h)^2}(\pi-\omega h)}$	same as $h\to0$

TABLE 3.2
Amplitudes of leading mean errors when $h \to 0$ and (separately) $\varepsilon \to 0$.

$$s_{j=0}(x) = \frac{\cos\omega x}{1+\hat{\phi}^{-1}(\omega)\left[\hat{\phi}(\omega+\frac{2\pi}{h})+\hat{\phi}(\omega-\frac{2\pi}{h})\right]}$$

$$= \cos\omega x\,(1-g_h(\omega,\varepsilon,h)) \qquad h\to0 \qquad (3.4)$$

$$= \cos\omega x\,(1-g_\varepsilon(\omega,\varepsilon,h)) \qquad \varepsilon\to0\,, \qquad (3.5)$$

recalling that $\hat{\phi}$ is also a function of ε. These two error functions for different $\phi(r)$ are summarized in Table 3.2.

The error clearly depends directly on the smoothness of the RBFs. For example for the radial function $\phi(r) = r^3$, with a discontinuity in the third derivative at the origin (recalling that $\phi(r)$ for $r \geq 0$ is extended symmetrically to $r \leq 0$) the converges becomes $O(h^4)$, whereas for $\phi(r) = r^2 \ln r$ (with a discontinuity in the second derivative), it becomes $O(h^3)$, i.e. in both cases *algebraic* convergence. For the cases of IQ and MQ, we see *spectral* convergence of the interpolant both as $h \to 0$ and as $\varepsilon \to 0$. MQ converge faster than IQ when $h \to 0$ since its error expression contains an additional factor of $h^{3/2}$. GA gives a much faster convergence still - of the form $O(e^{-\text{const}/h^2})$ rather than $O(e^{-\text{const}/h})$. We will denote this *super-spectral* convergence.

In the past, the regime of $\varepsilon \to 0$ was numerically inaccessible (in cases of scattered, multivariate data) due to the ill-conditioning of the linear system that leads to the expansion coefficients λ_k. The Contour-Padé method by Fornberg and Wright [8] has recently changed that, allowing numerically stable computations even in the limit of $\varepsilon \to 0$. Although the method (in its current form) is not practical for large data sets (more than about a hundred points), it has nevertheless conclusively demonstrated that numerical ill-conditioning as $\varepsilon \to 0$ is not an intrinsic problem for RBF interpolants, but instead is merely an undesirable artifact of a particular traditional approach to compute RBF interpolants. The difficulty of working numerically with small ε is technical rather than fundamental in nature.

4. Approximation of the first derivative at grid points. Knowing the RBF interpolation errors in cases of trigonometric data, we can explore how well derivatives are approximated.

4.1. Analysis for FD schemes. We start by illustrating in Fourier space the standard second order centered FD approximation (abbreviated FD2). When a basic Fourier mode $e^{i\omega x}$ is differentiated analytically, the result becomes $\frac{d}{dx} e^{i\omega x} = i\,\omega\,e^{i\omega x}$. Ignoring the "$i$", the factor that emerges in front of the exponential is $f_{exact}(\omega) = \omega$. Using FD2

$$\frac{d}{dx} e^{i\omega x} \approx \frac{\frac{1}{2}\left(e^{i\omega(x+h)} - e^{i\omega(x-h)}\right)}{h} = i\,\frac{\sin\omega h}{h}\,e^{i\omega x}$$

and we find

$$f_{FD2}(\omega) = \frac{\sin\omega h}{h}.$$

On an equi-spaced grid over $[-\pi, \pi]$ with spacing h, the range of Fourier modes that can be represented is $\omega \in [-\frac{\pi}{h}, \frac{\pi}{h}]$. That makes it natural to plot hf against $h\omega$ over the domain $[-\pi, \pi]$ or, noting that hf is an odd function of $h\omega$, over the domain $[0, \pi]$. The curve marked FD2 in Figure 4.1 a shows $hf_{FD2}(\omega)$. We can see that only a small fraction of modes near the origin are treated reasonably well (compared against the exact result - dotted straight line). The formal order of accuracy of the FD2 scheme can be read off from the level of fit at the origin:

$$h\,f_{FD2}(\omega) = \sin\omega h = \omega h - \frac{1}{6}(\omega h)^3 + \dots\;,$$

showing that only powers up to second order are correct. Similarly, we obtain

$$h\,f_{FD4}(\omega) = \frac{4}{3}\sin\omega h - \frac{1}{6}\sin 2\omega h = \omega h - \frac{1}{30}(\omega h)^5 + \dots,$$

etc. Figure 4.1 a shows also this function, as well as the corresponding ones for FD schemes up to order 10.

A cubic B-spline on a unit-spaced grid takes, at its three non-zero nodes, the values

first derivative values	$\frac{1}{2}$	0	$\frac{1}{2}$
function values	$\frac{1}{6}$	$\frac{2}{3}$	$\frac{1}{6}$

From this follows the function $hf_{CS}(\omega)$ for the derivatives computed from an interpolating cubic spline. It becomes

$$h\,f_{CS}(\omega) = i\,\frac{\frac{1}{2}e^{-i\omega h} + 0e^{0i\omega h} - \frac{1}{2}e^{i\omega h}}{\frac{1}{6}e^{-i\omega h} + \frac{2}{3}e^{0i\omega h} + \frac{1}{6}e^{i\omega h}} = \frac{3\,\sin\omega h}{2 + \cos\omega h} = \omega h - \frac{1}{180}(\omega h)^5 + \dots \quad (4.1)$$

Figure 4.1 a includes hf also for this cubic spline method (denoted CS4, since (4.1) shows it to be fourth order accurate). We can see that order alone does not tell the full story about the accuracy of a scheme - the (global) spline-based CS4 method holds its own very well against for example the FD6 scheme in the sense of providing good approximations over a wide frequency range.

4.2. Analysis for the piecewise smooth RBF schemes. The starting point is now equation (3.2). For $x_k = kh$, $k \in Z$, the interpolant reduces to

$$s(x_k) = \frac{e^{i\omega x_k}}{h\Xi(\omega, h)} \sum_{j=-\infty}^{\infty} \hat{\phi}\left(\omega + \frac{2\pi j}{h}\right) = e^{i\omega x_k}$$

a. FD2,...,FD10 (solid) and CS4 (dashed)　　　b. $\phi(r) = r^{2n-1}$ (solid) and $\phi(r) = r^{2n}\ln r$ (dashed)
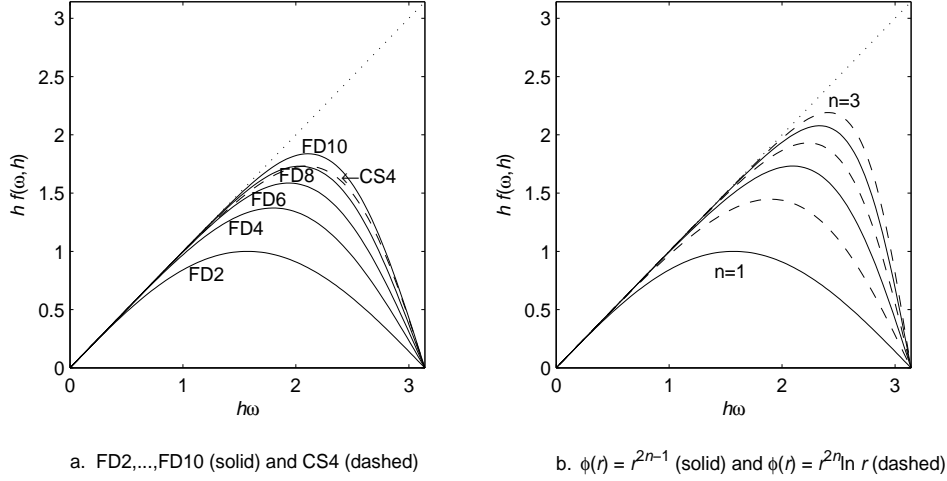
FIG. 4.1. *hf plotted against $h\omega$ for (a) centered FD methods and the cubic spline method, and (b) RBF approximations based on the radial functions $\phi(r) = r^{2n-1}$ (dashed) and $\phi(r) = r^{2n}\ln r$ (solid).*

(as should be expected, since the interpolation is exact at the nodes). The first derivative at the node points becomes

$$s'(x_k) = i \, \frac{e^{i\omega x_k}}{h\Xi(\omega,h)} \sum_{j=-\infty}^{\infty} (\omega + \frac{2\pi j}{h}) \, \hat{\phi}(\omega + \frac{2\pi j}{h}),$$

i.e.

$$f(\omega,h) = \frac{s'(x_k)}{i \, s(x_k)} = \frac{\sum_{j=-\infty}^{\infty} (\omega + \frac{2\pi j}{h}) \, \hat{\phi}(\omega + \frac{2\pi j}{h})}{\sum_{j=-\infty}^{\infty} \hat{\phi}(\omega + \frac{2\pi j}{h})}, \qquad (4.2)$$

where the denominator is equal to $h\Xi(\omega,h)$.

In the case of $\phi(r) = r^{2n-1}$, (4.2) becomes

$$h \, f_{r^{2n-1}}(\omega,h) = \frac{\sum_{j=-\infty}^{\infty} \frac{1}{(\omega+\frac{2\pi j}{h})^{2n-1}}}{\sum_{j=-\infty}^{\infty} \frac{1}{(\omega+\frac{2\pi j}{h})^{2n}}} = -h(2n-1) \frac{\frac{d^{2n-2}}{d\omega^{2n-2}} \cot(\frac{\omega h}{2})}{\frac{d^{2n-1}}{d\omega^{2n-1}} \cot(\frac{\omega h}{2})}.$$

For some low values of n, this simplifies to

$$
\begin{array}{llll}
n=1 & hf = & \sin \omega h & = \omega h - \frac{1}{6}(\omega h)^3 + \ldots \\
2 & hf = & \frac{3 \sin \omega h}{2 + \cos \omega h} & = \omega h - \frac{1}{180}(\omega h)^5 + \ldots \\
3 & hf = & \frac{50 \, \sin \omega h + 5 \sin 2\omega h}{33 + 26 \cos \omega h + \cos 2\omega h} & = \omega h - \frac{1}{5040}(\omega h)^7 + \ldots \\
\cdots & \cdots & &
\end{array}
$$

For the cubic case $\phi(r) = r^3$ ($n = 2$), we recover (4.1) for cubic splines. More generally (on a periodic domain), RBFs based on $\phi(r) = r^{2n-1}$ and splines of order $2n - 1$ give identical interpolants.

In the case of $\phi(r) = r^{2n} \ln r$, the general expression for hf becomes similarly

$$h \, f_{r^{2n}\ln r}(\omega,h) = \frac{\sum_{j=-\infty}^{\infty} \frac{1}{\left|\omega+\frac{2\pi j}{h}\right|^{2n}}}{\sum_{j=-\infty}^{\infty} \frac{1}{\left|\omega+\frac{2\pi j}{h}\right|^{2n+1}}} = -4n\pi \frac{\Psi^{(2n-1)}(\frac{\omega h}{2\pi}) - \Psi^{(2n-1)}(1 - \frac{\omega h}{2\pi})}{\Psi^{(2n)}(\frac{\omega h}{2\pi}) + \Psi^{(2n)}(1 - \frac{\omega h}{2\pi})},$$

10

a. IQ: $\omega = 1$, different ε b. IQ: $\varepsilon = 0.1$, different ω
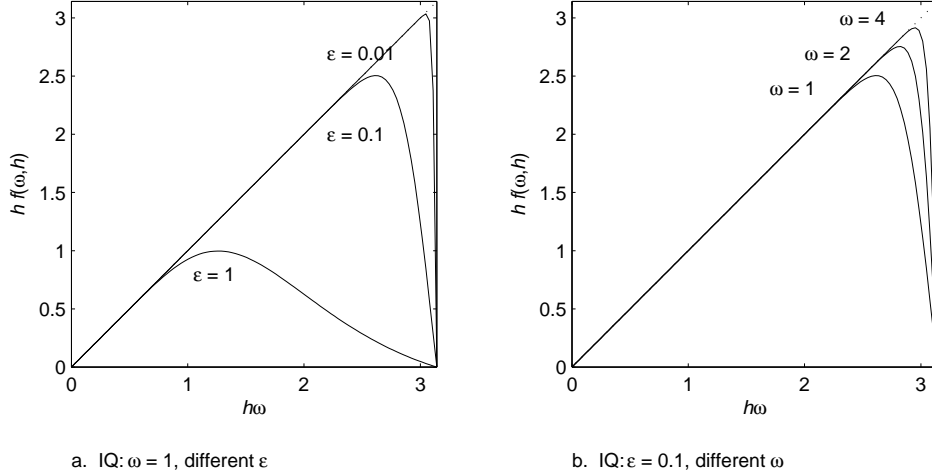
FIG. 4.2. *hf vs. $h\omega$ for IQ RBFs in the cases of (a) $\omega = 1$ and different ε, and (b) $\varepsilon = 0.1$ and different ω.*

which for some low values of n becomes

$$
\begin{array}{lll}
n = 1 & hf = & -4\pi \dfrac{\Psi^{(1)}\left(\frac{\omega h}{2\pi}\right) - \Psi^{(1)}\left(1 - \frac{\omega h}{2\pi}\right)}{\Psi^{(2)}\left(\frac{\omega h}{2\pi}\right) + \Psi^{(2)}\left(1 - \frac{\omega h}{2\pi}\right)} = \omega h + \dfrac{3\Psi^{(2)}(1)}{8\pi^3}(\omega h)^4 + \ldots \\[3ex]
\quad 2 & hf = & -8\pi \dfrac{\Psi^{(3)}\left(\frac{\omega h}{2\pi}\right) - \Psi^{(3)}\left(1 - \frac{\omega h}{2\pi}\right)}{\Psi^{(4)}\left(\frac{\omega h}{2\pi}\right) + \Psi^{(4)}\left(1 - \frac{\omega h}{2\pi}\right)} = \omega h + \dfrac{5\Psi^{(4)}(1)}{384\pi^5}(\omega h)^6 + \ldots \\[3ex]
\quad 3 & hf = & -12\pi \dfrac{\Psi^{(5)}\left(\frac{\omega h}{2\pi}\right) - \Psi^{(5)}\left(1 - \frac{\omega h}{2\pi}\right)}{\Psi^{(6)}\left(\frac{\omega h}{2\pi}\right) + \Psi^{(6)}\left(1 - \frac{\omega h}{2\pi}\right)} = \omega h + \dfrac{7\Psi^{(6)}(1)}{46080\pi^7}(\omega h)^8 + \ldots \\[2ex]
\quad \cdots & \cdots &
\end{array}
$$

As before, $\Psi^{(n)}(z) = \frac{d^{n+1}}{dz^{n+1}} \ln \Gamma(z)$ denotes the polygamma function. We can note that $\Psi^{(2n)}(1)$ are negative for all positive integers n. Like for $\phi(r) = r^{2n-1}$, $hf < h\omega$ for $0 < h\omega \leq \pi$.

Figure 4.1 b compares hf against $h\omega$ in the cases of $\phi(r) = r^{2n-1}$ and $\phi(r) = r^{2n} \ln r$. The accuracy improves with increasing values of n, giving derivative approximations of order $2n$ for $\phi(r) = r^{2n-1}$ and of order $2n + 1$ for $\phi(r) = r^{2n} \ln r$. For the same value of n, the accuracies differ by one order (just as was the case for interpolants, as was seen from the $g_h(\omega, \varepsilon, h)$ functions in Table 3.2).

4.3. Analysis for RBF schemes with $\phi(r)$ infinitely differentiable. A new aspect enters in the analysis when $\phi(r)$ is infinitely differentiable. Not only does the shape parameter ε introduce an additional length scale, the variables ω and h in $f(\omega, h)$ will no longer appear only in the form of the product ωh. As an example, for the IQ case, $\phi(r) = 1/(1 + (\varepsilon r)^2)$, we can obtain from (4.2)

$$
h\, f_{IQ}(\omega, h) = \omega h - \frac{\pi \, \sinh \frac{\omega}{\varepsilon}}{\sinh \frac{\pi}{h\varepsilon} \, \cosh \left(\frac{\pi}{h\varepsilon} - \frac{\omega}{\varepsilon}\right)} = \omega h - 2\pi (e^{2\omega/\varepsilon} - 1)\, e^{-\frac{2\pi}{\varepsilon h}} + \ldots \ .
$$

The exponential decay of the error as $h \to 0$ (ω fixed) signifies its spectral accuracy.

For the cases of MQ and GA, there do not appear to be any simple closed-form expressions available for $hf(\omega, h)$, but the functions can be readily computed from (4.2) and displayed graphically. In previous cases (with piecewise smooth $\phi(r)$), each

11

a. ω = 1, ε = 1.0   b. ω = 1, ε = 0.1
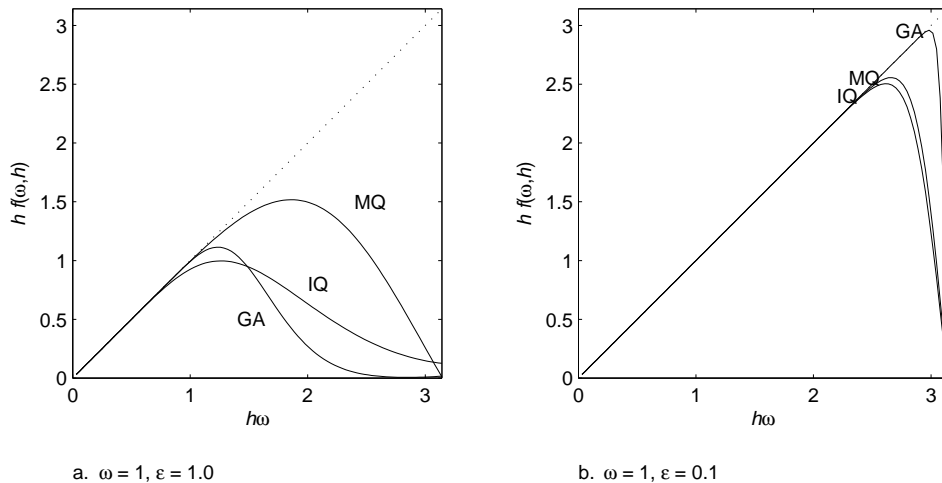
FIG. 4.3. *hf vs. hω displayed for IQ, MQ, and GA in the case of ω = 1 and (a) ε = 1.0 , (b) ε = 0.1.*

method was fully described by one single curve in the $hf(\omega, h)$ against $h\omega$ plots. In these cases with $\phi(r)$ infinitely differentiable, we need to draw different curves not only for different values of ε, but also for different values of ω. Figures 4.2 a and b show $hf(\omega, h)$ against $h\omega$ in the IQ cases of $\{\omega = 1,$ different $\varepsilon\}$ and $\{\varepsilon = 0.1,$ different $\omega\}$, respectively.

In Figure 4.3 a, b the three main types of infinitely smooth RBFs that are considered in this study (IQ, MQ, and GA), are compared against each other for the case of $\omega = 1$ and $\varepsilon = 1.0$ and $\varepsilon = 0.1$, respectively. For $\varepsilon = 1.0$ we see the high formal order of accuracy by the accuracy of the fit to the exact solution near the origin, but the treatment of high frequencies is not much better than with typical FD methods. This case ($\varepsilon = 1.0$, with the basis functions not particularly flat), is probably typical of the regime in which RBFs are often used. MQ is here clearly the most attractive choice of the three we are considering. For $\varepsilon = 0.1$ we have reached a different regime, and the accuracies are far higher. The advantage of MQ over IQ is now rather slim (due to the extra factor of $h^{1/2}$ for $g_\varepsilon(\omega, \varepsilon, h)$ noted in Table 3.2). More noticeable is the strength of the GA method. However, since all the three methods offer excellent accuracy over almost all the wave modes that are present, the practical advantage of the GA method's super-spectral accuracy (both as $h \to 0$ and $\varepsilon \to 0$) remains unclear.

5. Conclusions. The main strength of RBF interpolants lie in their flexibility, convenience, and accuracy when applied to scattered multi-dimensional data sets. In such a general setting, errors can be computed numerically, but analytic error analysis is often difficult or impractical (although notable such estimates have been achieved, e.g. [17], [18], [20]). By considering the simplified case of equi-spaced periodic data, we have been able to obtain a number of novel closed-form expressions, as well as estimates of errors which support previously observed convergence properties. In particular, we have described how the errors decrease for very smooth functions when we increase the number of node points ($h \to 0$) and when the basis functions are made increasingly flat ($\varepsilon \to 0$). The closed-form error expressions show how the errors for different RBFs fall in three categories - algebraic, spectral, and super-spectral - dependent on the decay rates of the Fourier transform of the radial function. The

limit of $\varepsilon \to 0$ is of particular theoretical interest because (excepting rare special cases)

- 1-D: Over a finite set of arbitrarily spaced nodes, the limiting interpolant becomes identical to the standard Lagrange's interpolation polynomial [5], and
- n-D: The limit becomes a low-degree multivariate interpolation polynomial [9].

This demonstrates that, in the $\varepsilon \to 0$ limit, RBF methods reproduce traditional spectral methods, such as Chebyshev, Fourier, etc. Not only have spectral methods become generalized to unstructured node sets in arbitrary domains, we have also obtained the option in spectral methods of not proceeding all the way into the $\varepsilon \to 0$ limit. Many challenges remain in the area of RBF analysis. To mention just a couple:

- Generalize the full range of the present 1-D equispaced results to irregular node situations in more dimensions, and
- Understand the generality and utility of super-spectral convergence.

REFERENCES

[1] M. D. Buhmann, *Radial Basis Functions*, Cambridge University Press (2003).
[2] M. D. Buhmann and N. Dyn, Spectral convergence of multiquadric interpolation, in *Multivariate Approximation: From CAGD to Wavelets*, K. Jetter and F.I. Utreras (eds), World Scientific, Singapore (1993), 35-75.
[3] M. D. Buhmann and M. J. D. Powell, Radial basis function interpolation on an infinite regular grid, in *Algorithms for Approximation II*, M. G. Cox and J. C. Mason (eds), Chapman & Hall, London, 1990, 146-169.
[4] R.E. Carlson and T.A. Foley, The parameter R^2 in multiquadric interpolation, *Comput. Math. Appl.* 21 (1991), 29-42.
[5] T.A. Driscoll and B. Fornberg, Interpolation in the limit of increasingly flat radial basis functions, *Comput. Math. Appl.*, 43 (2002), 413-422.
[6] T.A. Foley, Near optimal parameter selection for multiquadric interpolation, *J. Appl. Sci. Comput.* 1 (1994), 54-69.
[7] B. Fornberg, *A Practical Guide to Pseudospectral Methods*, Cambridge University Press, 1996.
[8] B. Fornberg and G. Wright, Stable computation of multiquadric interpolants for all values of the shape parameter, to appear *Comput. Math. Appl.* (2004).
[9] B. Fornberg, G. Wright and E. Larsson, Some observations regarding interpolants in the limit of flat radial basis functions, to appear *Comput. Math. Appl.*, (2003).
[10] K. Jetter, Multivariate approximation from the cardinal point of view, in *Approximation Theory VII*, E.W. Cheney, C.K. Chui and L.L. Schumaker (eds), Academic Press 1992, 131-161.
[11] D.S. Jones, *Generalized Functions*, McGraw-Hill, New York, 1966.
[12] E.J. Kansa, A scattered data approximation scheme with applications to computational fluid dynamics. I. Surface approximations and partial derivative estimates, *Comput. Math. Appl.* 19 (8/9) (1990), 127-145.
[13] E.J. Kansa, Multiquadrics - A scattered data approximation scheme with applications to computational fluid dynamics. II. Solutions to parabolic, hyperbolic and elliptic partial differential equations, *Comput. Math. Appl.* 19 (8/9) (1990), 147-161.
[14] E. Larsson and B. Fornberg, A numerical study of radial basis function based solution methods for elliptic PDEs, Computers and Mathematics with Applications, 46 (2003), 891-902.
[15] Lighthill, M.J., *Fourier Analysis and Generalised Functions*, Cambridge University Press, 1958.
[16] W.R. Madych, Miscellaneous error bounds for multiquadric and related interpolators, *Comput. Math. Appl.*, 24 (1992), 121-138.
[17] W.R. Madych and S.A. Nelson, Multivariate interpolation and conditionally positive functions I, *Approx. Theory Appl.*, 4 (1988), 77-89.
[18] W.R. Madych and S.A. Nelson, Multivariate interpolation and conditionally positive functions II, *Approx. Theory Appl.*, 4Math. Comp. 54 (1990), 211-230.
[19] S. Rippa, An algorithm for selecting a good value for the parameter c in radial basis function interpolation, *Adv. Comput. Math.* 11 (1999), 193-210.

[20] J. Yoon, Spectral approximation orders of radial basis function interpolation on the Sobolev space, *SIAM J. Math. Anal.* 33 (4) (2001), 946-958.